Article

# Catalytic asymmetric synthesis of *meta* benzene isosteres

https://doi.org/10.1038/s41586-024-07865-4

Received: 4 March 2024

Accepted: 22 July 2024

Published online: 21 August 2024

Check for updates

Mingkai Zhang[1], Matthew Chapman[1], Bhagyesh R. Sarode[2], Bingcong Xiong[1], Hao Liang[1], James K. Chen[2,3,4]✉, Eranthie Weerapana[1]✉ & James P. Morken[1]✉

Although aromatic rings are common elements in pharmaceutically active compounds, the presence of these motifs brings several liabilities with respect to the developability of a drug[1]. Nonoptimal potency, metabolic stability, solubility and lipophilicity in pharmaceutical compounds can be improved by replacing aromatic rings with non-aromatic isosteric motifs[2]. Moreover, whereas aromatic rings are planar and lack three-dimensionality, the binding pockets of most pharmaceutical targets are chiral. Thus, the stereochemical configuration of the isosteric replacements may offer an added opportunity to improve the affinity of derived ligands for target receptors. A notable impediment to this approach is the lack of simple and scalable catalytic enantioselective syntheses of candidate isosteres from readily available precursors. Here we present a previously unknown palladium-catalysed reaction that converts hydrocarbon-derived precursors to chiral boron-containing nortricyclanes and we show that the shape of these nortricyclanes makes them plausible isosteres for *meta* disubstituted aromatic rings. With chiral catalysts, the Pd-catalysed reaction can be accomplished in an enantioselective fashion and subsequent transformation of the boron group provides access to a broad array of structures. We also show that the incorporation of nortricyclanes into pharmaceutical motifs can result in improved biophysical properties along with stereochemistry-dependent activity. We anticipate that these features, coupled with the simple, inexpensive synthesis of the functionalized nortricyclane scaffold, will render this platform a useful foundation for the assembly of new biologically active agents.

Bioactive compounds, from natural products to clinically relevant active ingredients, often contain aromatic rings. The reasons for incorporation of this motif are multifold[1]: (1) the rigidity of aromatic rings often restricts available molecular conformations thereby lessening the entropic cost for the aromatic ligand to bind to a target receptor; (2) aromatic rings participate in unique non-covalent interactions that can provide enhanced attraction to receptor binding pockets; and (3) the methods used to attach substituents to aromatic rings include efficient cross-coupling reactions[3] that facilitate construction and screening of diverse compound collections. These notable benefits are counter-balanced by the ready oxidation of π-electron-rich aromatic rings that can severely diminish metabolic stability[4]. Moreover, relative to their C($sp^3$) counterparts, aromatic molecules have decreased aqueous solubility[5] and increased log *D* (ref. 6). A particular challenge arising from the increased lipophilicity of an aromatic compound is that this feature increases off-target promiscuity[7] that is problematic for drug development. To address this limitation, bicyclic hydrocarbon frameworks have been advanced as C($sp^3$)-based isosteric replacements for aromatic rings[8], with the expectation that the saturated bicyclic analogues might offer enhanced biophyscial properties while retaining biological activity[9]. When appropriately designed, these molecular scaffolds can retain the conformational restriction of the benzenoid ring while simultaneously avoiding associated liabilities. Following this model, an array of small bicyclic motifs have been developed that position substituents at a similar distance and with similar exit vectors compared with substituted arenes, with selected examples of *meta* benzene isosteres shown in Fig. 1a (refs. 10–22).

In the context of ligand development, two important features arise when planar C($sp^2$)-based aromatic rings are replaced with C($sp^3$)-based bicyclic isosteres. The first is that of retaining the efficient, reliable, modular and scalable synthesis techniques that accompany modern catalytic cross-coupling methods. The second issue is that of three-dimensional shape. Even if the isostere positions its substituents in a manner that would superimpose them onto those of an aromatic nucleus, the tetrahedral nature of the saturated carbon centres in the isostere automatically results in a three-dimensionality that is absent from the flat aromatic ring system. As the preponderance of biologically relevant receptors are chiral, the handedness of a nonsymmetric isostere may either enhance or impede the binding of the derived ligand to its cognate receptor[18,23]. The way MK-5108 binds to the inactive DFG-out

[1]Department of Chemistry, Boston College, Chestnut Hill, MA, USA. [2]Department of Chemical and Systems Biology, Stanford University, Stanford, CA, USA. [3]Department of Developmental Biology, Stanford University, Stanford, CA, USA. [4]Department of Chemistry, Stanford University, Stanford, CA, USA. ✉e-mail: jameschen@stanford.edu; eranthie.weerapana@bc.edu; morken@bc.edu

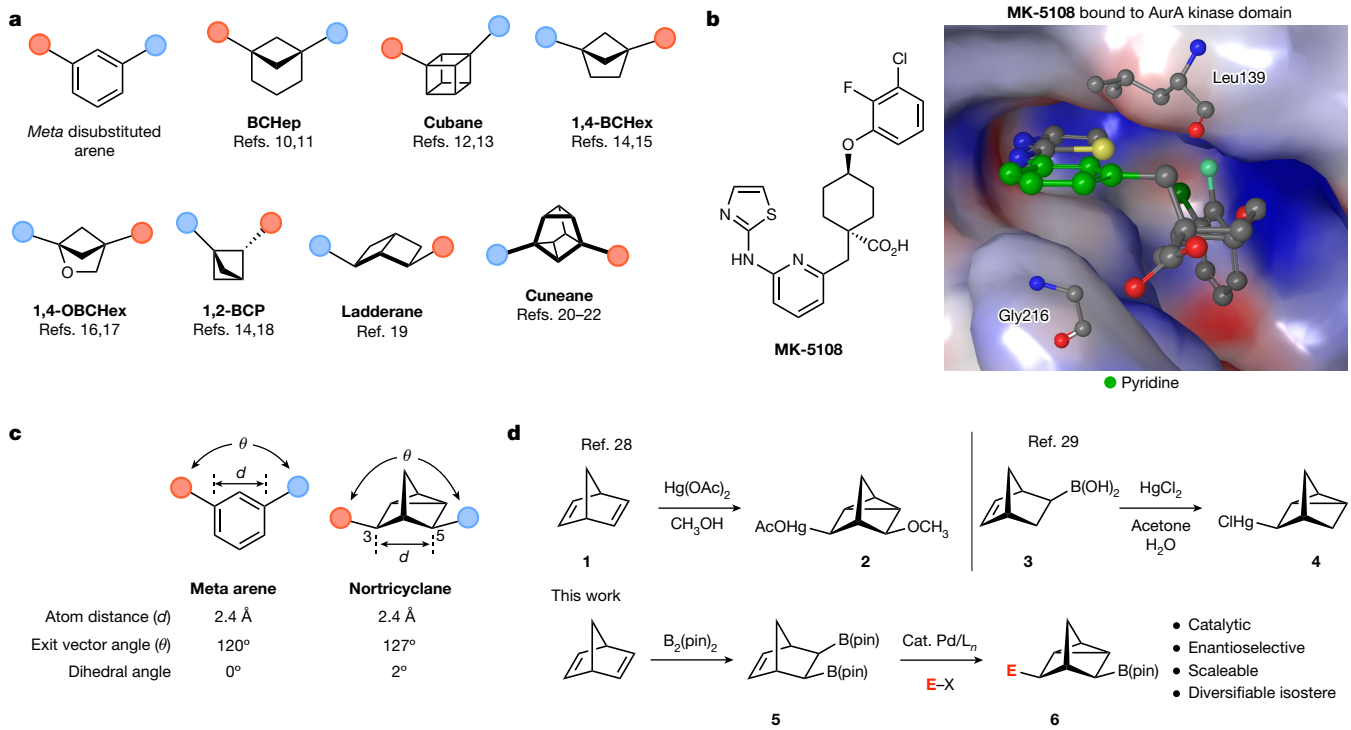


**Fig. 1 | Saturated bicycloalkanes as isosteric replacements for aromatic rings. a**, Selected recent examples of *meta* benzene isosteres. **b**, The kinase inhibitor MK-5108 bound to the chiral binding pocket in the kinase domain of AurA. **c**, Structural comparison of a *meta* disubstituted arene and a 3,5-disubstituted nortricyclane. **d**, Metal-promoted reactions for the construction of nortricyclanes from simple bicycloheptane precursors. pin, pinacolato group.

state of the mitotic kinase Aurora A is illustrative[24,25]. When bound, the *meta* disubstituted arene in MK-5108 is sandwiched in a hydrophobic pocket with Leu139 positioned 3.9 Å above the arene (carbon-to-carbon distance) and Gly216 3.5 Å below (Fig. 1b). Thus, when a nonsymmetric benzene isostere occupies this binding pocket, it would be expected to fit better if it occupies more volume in the upper region of the receptor rather than the lower. Such a lock-and-key fit of ligands to their complementary receptors can result in enhanced specificity and ligand promiscuity has been shown to diminish as the number of chiral centres in a compound increases[7]. From this vantage point, it is clear that methods are needed to control the absolute configuration of the overall molecular ensemble. In this report, we describe a reaction that retains all the practical advantages of contemporary cross-coupling and that allows conversion of simple starting materials into enantiomerically enriched 3,5-disubstituted nortricyclane frameworks (Fig. 1c). Of note, comparison of the metrical parameters of the nortricyclane with those of benzene show that carbons 3 and 5 are equidistant with the *meta* carbons of benzene. Moreover, the exit vectors for connection to substituents at carbons 3 and 5 have an angle between them that is nearly the same as in benzene (127° versus 120°), and the vectors are essentially co-planar as in the aromatic framework. Last, the process that we describe for the production of 3,5-disubstituted nortricyclanes occurs by a heretofore unknown catalytic reaction. This reaction occurs with low loadings of a chiral palladium complex and delivers malleable boron-containing isosteres, holding marked potential for further modification.

The bicyclic norbornadiene skeleton (**1**; Fig. 1d) has provided an instructive framework for studying the nature of non-classical carbocations and for probing the ability of homoconjugation to stabilize organic structures and influence the course of their chemical reactions[26,27]. Owing to the through-space interaction between the two π-bonds, the conversion of the bicyclo[2.2.1] framework to nortricyclanes (that is, **2**) readily occurs on the addition of suitable electrophilic reagents[28]. Similar electrophilic activation of bicyclic organometallics (that is, **3**) can result in ring-closing C–C bond formation to furnish the nortricyclane skeleton (**4**) (ref. 29). In contrast to these stoichiometric reactions, we herein demonstrate that a catalytic synthesis of nortricyclanes operates when the mercury salts used in the synthesis of **2** and **4** are replaced with substoichiometric quantities of palladium complexes in conjunction with an organic electrophile. The reaction that occurs results in ring closure with the concomitant addition of the organic electrophile to the bicyclic framework. An important finding for the application of this reaction to the modular construction of enantiomerically enriched *meta* benzene isosteres is that the cyclization occurs with *meso* diboron substrate **5**, a compound that is shelf-stable and readily available on a multigram scale. Reaction of **5** delivers a nortricyclane **6** that retains one boronic ester functional group, apart from the newly appended organic substituent (E). After optimization of the reaction (conditions, ligand structure), it was found that a wide array of enantiomerically enriched boron-containing nortricyclanes can be prepared in excellent yield and enantioselectivity.

## Development of the Pd-catalysed reaction

In the presence of catalytic quantities of $Pd(OAc)_2$ and chiral biarylmonophosphine ligand **L1** (ref. 30) (Fig. 2), diboron substrate **5** and organic electrophiles engage in catalytic enantioselective ring closure to nortricyclanes. With simple substituted aryl bromides, the reaction occurs in high yield and enantioselectivity. The products from both electron-deficient (**11, 12**) and electron-rich (**13, 15**) electrophiles can be readily obtained, although selectivity is diminished with a strong electron-withdrawing nitroarene electrophile (**16**). Also of note, heterocyclic electrophiles were found to engage in the reaction (products **20**–**23**). With respect to practical features, it merits mention that unprotected anilines and phenols do not seem to interfere

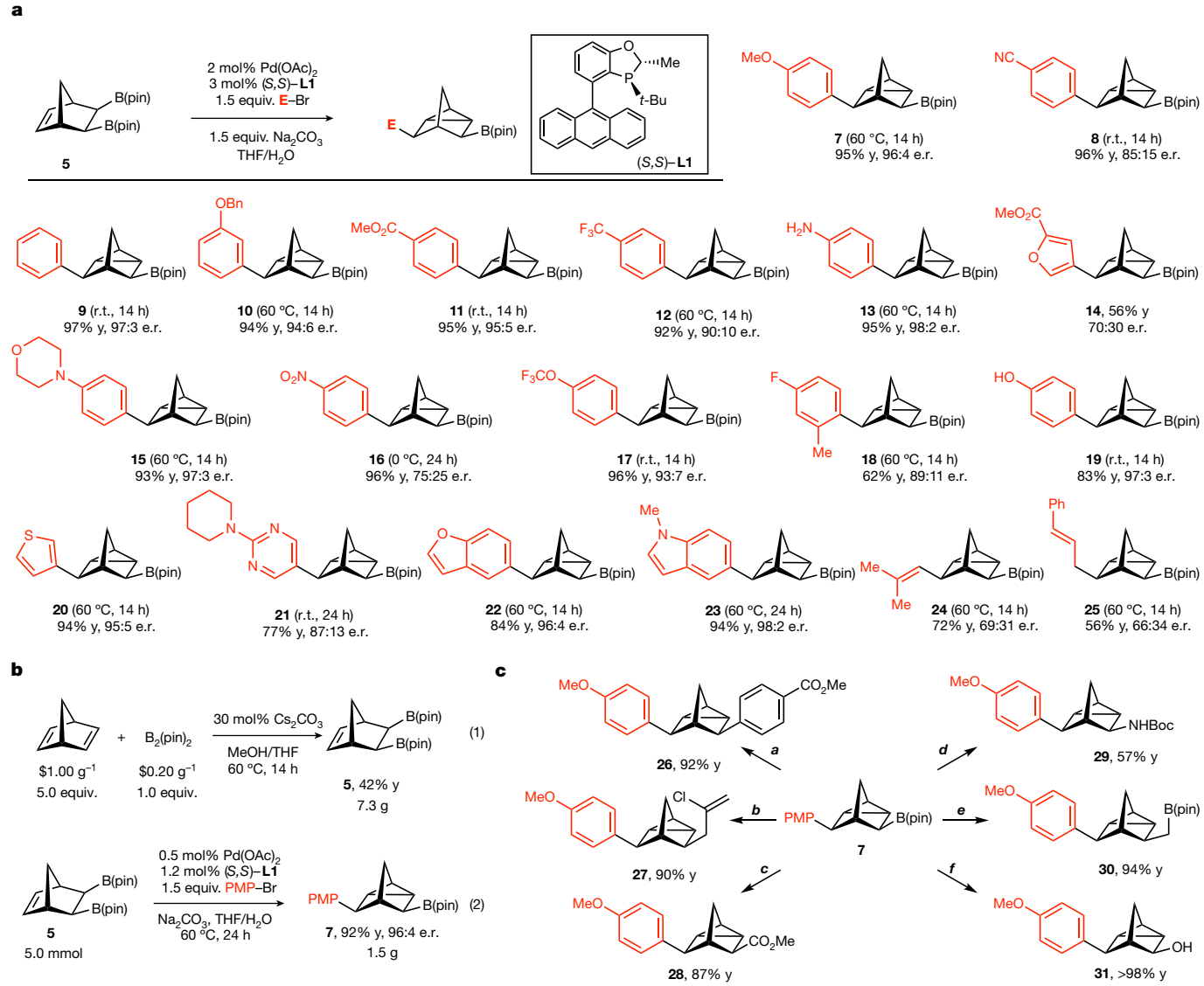


**Fig. 2 | Pd-catalysed enantioselective construction of chiral nortricyclanes and their applications. a**, Enantioselective coupling of **5** with electrophiles. Yields (y) are isolated yields of the purified products. The enantiomeric ratio (e.r.) was determined by supercritical fluid chromatography. Product **21** required 5 mol% catalyst; product **25** from cinnamyl chloride. Absolute configuration determined by X-ray analysis of compound **20**. Bn, benzyl; Ph, phenyl; PMP, *para*-methoxyphenyl; r.t., room temperature. **b**, Single-step multigram-scale synthesis of *meso* bis(boronate) substrate **5** and its conversion to **7**. The prices shown are from Ambeed for $B_2(pin)_2$ and Sigma-Aldrich for norbornadiene. **c**, Transformations of boron-containing nortricyclane **7**. Conditions: a: *t*-BuLi then $Zn(OAc)_2$; G3-PdCPhos, Ar-Br. b: *t*-BuLi, then 20 mol% CuCN, 2,3-dichloropropene. c: *t*-BuLi, then 20 mol% CuCN, methyl chloroformate. d: $MeONH_2$, *n*-BuLi; then $Boc_2O$. e: *n*-BuLi, $CH_2BrCl$. f: NaOH, $H_2O_2$.

with the process and that extension to non-aromatic electrophiles (**24, 25**) seems promising. Practical application of the nortricyclane synthesis necessitates procedures that operate on a large scale as well as functional group transformations that effectively replace the remaining boronic ester in the catalytic reaction product. With regards to the first aspect, it was found that the bis(boronate) substrate **5** could be prepared on a multigram scale directly from inexpensive commercially available norbornadiene and $B_2(pin)_2$ (Fig. 2b, (1)). The reaction of **5** could be conducted on a 5 mmol scale and, so long as the reaction time is extended to 24 h, could be accomplished in good yield with only 0.5 mol% of palladium complex (Fig. 2b, (2)). As the transformations in Fig. 2c indicate, the boronic ester in product **7** can be replaced stereospecifically by Zn-based catalytic cross-coupling[31] (**26**), Cu-catalysed allylation and carboxylation[32] (**27** and **28**), direct amination[33] (**29**), homologation[34] (**30**) or conversion to the derived alcohol (**31**).

## Study of reaction mechanism

Mechanistic experiments provide insight into a likely pathway that leads to the product from substrate-derived cyclic ate complex **32** (Fig. 3a), a compound that has precedent from previous studies in our lab[35,36]. The density functional theory calculations were used to determine the free energy profile of reaction paths originating from a palladium–olefin complex (**GS0**) that would be obtained by oxidative addition between LPd(0) and an electrophile, followed by association with **32**. In one route (path A, red), carbopalladation of the alkene (**TS1a**) delivers Pd(II) intermediate **GS1a**, which might then undergo an uncommon displacement of palladium(II) (refs. 37,38) by **TS2a** in which the organoboron serves as a nucleophile to simultaneously expel and reduce the metal. Alternatively (path B, blue), on binding to Pd(II), the alkene may become sufficiently electrophilic that nucleopalladation[39] by **TS1b** may generate **GS1b**, with direct reductive

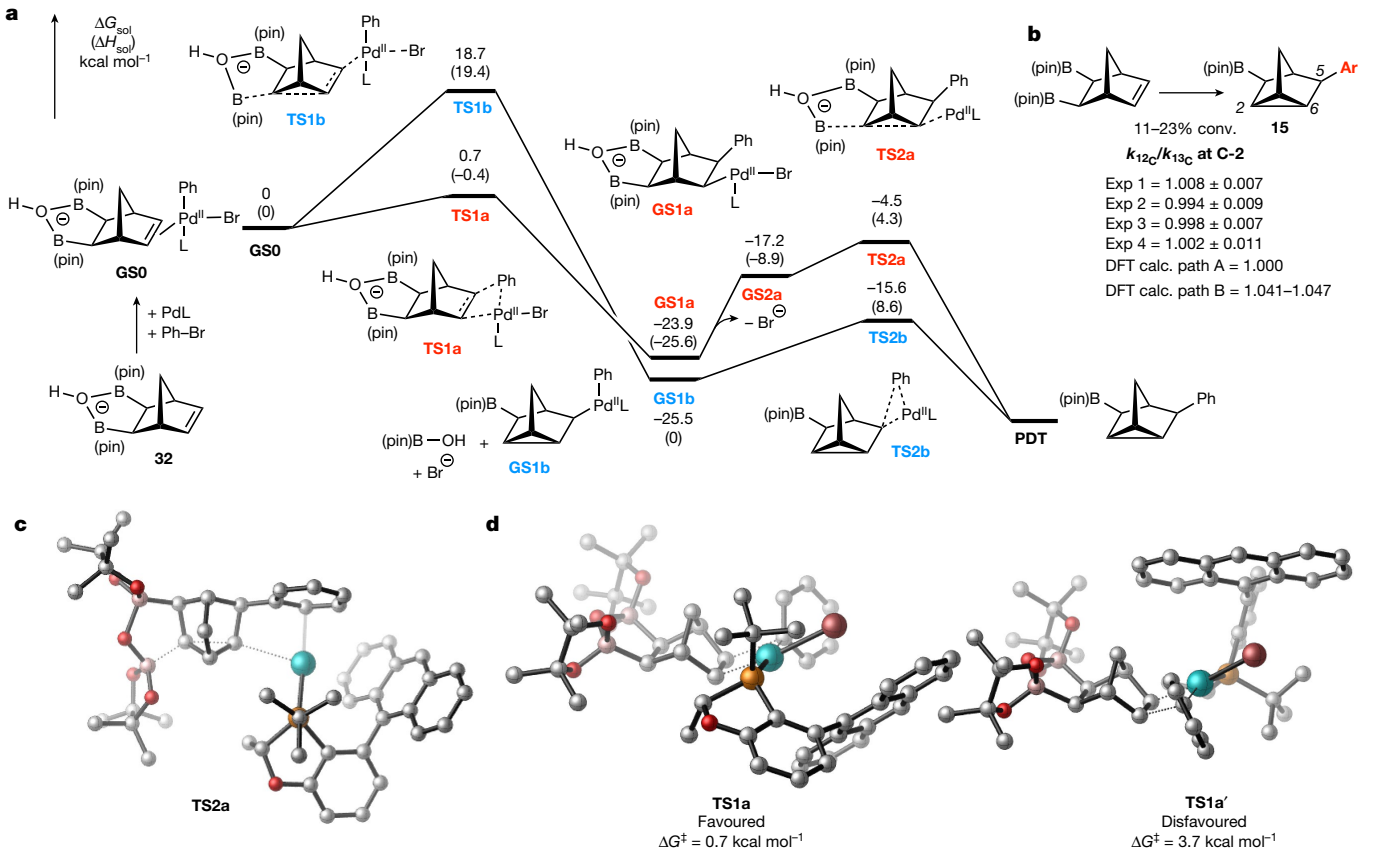


**Fig. 3 | Mechanistic aspects of the Pd-catalysed nortricyclane synthesis.** **a**, Calculated ground states and transition states for a carbopalladation-based mechanism (path A, red) and a nucleopalladation-based mechanism (path B, blue) for the Pd-catalysed synthesis of nortricyclanes. Methods: B3PW91(D3)/def2-TZVP/def2-TZVPP(Pd)/smd(THF)//B3LYP(D3BJ)/def2-SVP/def2-TZVP(Pd). **b**, Selected $^{13}C$ kinetic isotope effects as determined by the natural abundance isotope method of ref. 41. **c**, Calculated transition state geometry for TS2a. **d**, Calculated stereochemistry-determining transition states leading to the major and minor enantiomers of carbopalladation product. $\Delta G^{\ddagger}$, energy difference between the transition state and the reactants.

elimination then delivering the product. Calculations indicate that the carbopalladation pathway is lower in energy, with the olefin migratory insertion to give **GS1a** occurring by a much lower barrier compared with the nucleopalladation step (0.7 kcal mol$^{-1}$ versus 18.7 kcal mol$^{-1}$). From **GS1a**, dissociation of bromide allows the ring-closing reductive displacement of Pd(II) to occur with an accessible 19.4 kcal mol$^{-1}$ barrier by **TS2a** (Fig. 3c). Of note, calculation of the $^{13}C$ kinetic isotope effects that would arise from **TS1a** (ref. 40) matches well with those determined experimentally by the Singleton method[41] (Fig. 3b). Most notably, palladium-catalysed coupling of **5** exhibits a negligible KIE at C2, which is consistent with the carbopalladation-based mechanism but not the nucleopalladation pathway. Further mechanistic evidence in support of the carbopalladation pathway can be found in the Supplementary Information. According to these experiments, the carbopalladation step is enantio-determining and computational studies were undertaken to elucidate the origin of enantioinduction. As shown in Fig. 3d, the calculated structure of the transition state leading to the minor product stereoisomer places the $CH_2$ bridge of the bicycloheptane motif directly under the sterically encumbered anthracene ring system, whereas the conformation of the transition state for the major isomer avoids this interaction.

## Biophysical and biochemical properties

To determine whether nortricyclane frameworks are suited for use in bioactive molecules, both enantiomers of **33** were prepared as chiral isosteric analogues of the fatty acid amide hydrolase (FAAH) inhibitor URB597 (refs. 42,43) and subjected to analysis (Fig. 4a). Of note, although the isosteric analogues have similar molecular weight as URB597, they have 10-fold increased solubility in the aqueous buffer while maintaining comparable lipophilicity ($\alpha$ log $D$). Apart from these positive attributes, the isosteric analogues exhibit measurably increased metabolic stability relative to URB597 as determined by mouse liver microsomal assay. To probe for the effect of chirality on biological activity, compounds (*R*,*S*)-**33** and (*S*,*R*)-**33** were compared by quantitative activity-based protein profiling experiments (for complete details, see the Supplementary Information). Mouse-brain homogenates were treated with varying concentrations of each compound before exposure to the serine hydrolase-directed activity-based probe fluorophosphonate (FP)-biotin. FP-labelled proteins were enriched on streptavidin beads and analysed by quantitative tandem mass tagging (TMT)-based mass spectrometry[44]. Of note, although (*R*,*S*)-**33** and (*S*,*R*)-**33** were not as potent as URB597, the isosteric analogues retained the ability to inhibit FAAH and show different potencies: (*R*,*S*)-**33** exhibits an $IC_{50}$ of 0.50 μM, whereas that for (*S*,*R*)-**33** is more than 4 μM. Furthermore, the incorporation of the isosteres did not alter the proteome-wide selectivity of URB597, as both isosteres maintained high selectivity for FAAH over 23 other detected serine hydrolases.

In a second comparative analysis, the enantiomeric tricyclanes (*S*,*R*)-**34** and (*R*,*S*)-**34** were prepared as analogues of the Hedgehog (Hh) pathway[45] inhibitor, sonidegib[46] (Fig. 4b). Aberrant Hedgehog signalling has been implicated in certain types of cancer, and sonidegib inhibits activation of this pathway by interacting with the associated signal transducer, Smoothened (SMO). Comparison of stereoisomeric

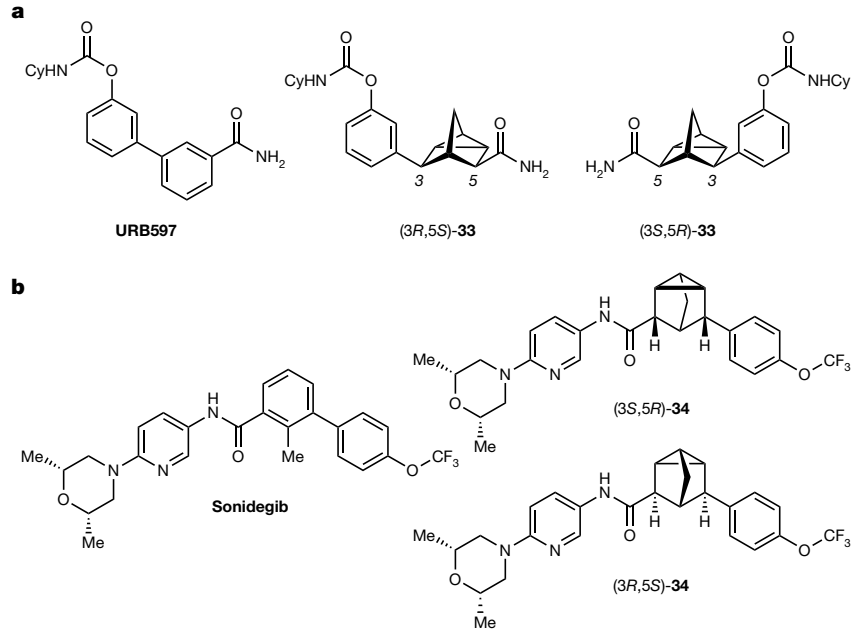


| | URB597 | (3*R*,5*S*)-**33** | (3*S*,5*R*)-**33** |
|---|---|---|---|
| MW (g mol$^{-1}$) | 338.4 | 354.4 | 354.4 |
| Kinetic solubility (μM)[a] | 1.01 | 12.66 | 10.16 |
| α log *D*[b] | 3.69 | 3.57 | 3.56 |
| Microsomal stability (% remaining)[c] | 37 | 67 | 75 |
| $IC_{50}$ FAAH (μM)[d] | 0.0114 | 0.50 | >4 |

| | Sonidegib | (3*S*,5*R*)-**34** | (3*R*,5*S*)-**34** |
|---|---|---|---|
| MW (g mol$^{-1}$) | 485.5 | 487.5 | 487.5 |
| Kinetic solubility (μM)[a] | 0.02 | 1.04 | 0.86 |
| α log *D*[b] | 5.74 | 5.62 | 5.61 |
| Microsomal stability (% remaining)[c] | 78 | 31 | 50 |
| $IC_{50}$ Hh (μM)[e] | 0.0036 | 0.50 | 0.20 |

**Fig. 4 | Pharmacokinetic analysis of nortricyclane-based analogues and their inhibitor activity against FAAH and Hedgehog signalling. a**, Analysis of the FAAH inhibitor URB597 and analogues (*R*,*S*)-**33** and (*S*,*R*)-**33**. **b**, Analysis of sonidegib and analogues (*S*,*R*)-**34** and (*R*,*S*)-**34**. [a]Determined in PBS buffer at pH = 7.4 after 24 h. [b]Defined as log *D* at pH = 7.4; determined by HPLC analysis. [c]Determined at 30 min in the presence of male CD-1 mouse liver microscomes with NADPH. [d]Inhibition of FAAH determined by quantitative mass spectrometry profiling. See the Supplementary Information for a complete dataset. [e]Inhibition of Hedgehog signalling in Shh-LIGHT2 cells. Data are an average of five replicates.

isosteres **34** was conducted by three independent $IC_{50}$ determinations using a dual luciferase assay in Shh-LIGHT2 cells[47], and it was found that the enantiomeric sonidegib analogues inhibit Hh signalling with submicromolar potencies ($IC_{50}$ = 0.50 μM and 0.20 μM for the (*S*,*R*)-**34** and (*R*,*S*)-**34**, respectively), and with a modest, at best (*P* = 0.26), difference in activity for the two stereoisomers. Overall, the preliminary analysis of the nortricyclane isosteres is in line with expectations: replacement of arenes with C($sp^3$)-based isosteres results in a 10-fold to 50-fold improvement in solubility, probably as a result of increased solvation of the C($sp^3$) analogues as suggested in refs. 48,49. Of note, the stereochemistry-dependent activity of nortricyclane isosteres (**33** and **34**) seems to reinforce the notion that shape matters when binding to biological targets, and it is notable that differences in activity are detected even with isosteric analogues that have not been reoptimized to bind their target receptors. We can anticipate that as chiral ligands are fine-tuned for affinity, the absolute stereochemistry of the isostere is likely to become increasingly important.

In summary, catalytic enantioselective nortricyclane synthesis provides an efficient entry into chiral *meta* benzene bioisosteres, and the chirality of the tricyclic motif plays a part in the shape-dependent binding of the derived ligands with their target receptors. The ease and robustness of the catalytic synthesis, combined with the biophysical properties of nortricyclanes should provide opportunities for pharmaceutical development. Although further exploration of the tricycloheptane skeleton seems warranted, further study of the unique catalytic process that leads to its formation—especially the C–C bond-forming reductive displacement of Pd(II)—may provide new strategies for reaction development.

## Online content

Any methods, additional references, Nature Portfolio reporting summaries, source data, extended data, supplementary information, acknowledgements, peer review information; details of author contributions and competing interests; and statements of data and code availability are available at https://doi.org/10.1038/s41586-024-07865-4.


1. Salomen, L. M., Ellermann, M. & Diederich, F. Aromatic rings in chemical and biological recognition: energetics and structures. *Angew. Chem. Int. Edn* **50**, 4808–4842 (2011).
2. Locke, G. M., Bernhard, S. S. R. & Senge, M. O. Nonconjugated hydrocarbons as rigid-linear motifs: isosteres for material sciences and bioorganic and medicinal chemistry. *Chem. Eur. J.* **25**, 4590–4647 (2019).
3. Nishihara, Y. (ed.) *Applied Cross-Coupling Reactions* Vol. 80 (Springer, 2013).
4. Dalvie, D., Nair, S., Kang, P. & Loi., C.-M. in *Metabolism, Pharmacokinetics and Toxicity of Functional Groups* (ed. Smith, D. A.) 275–327 (Royal Society of Chemistry, 2010).
5. Lovering, F., Bikker, J. & Humblet, C. Escape from flatland: increasing saturation as an approach to improving clinical success. *J. Med. Chem.* **52**, 6752–6756 (2009).
6. Ritchie, T. J. & Macdonald, S. F. J. The impact of aromatic ring count on compound developability—are too many aromatic rings a liability in drug design? *Drug Discov. Today* **14**, 1011–1020 (2009).
7. Lovering, F. Escape from Flatland 2: complexity and promiscuity. *Med. Chem. Commun.* **4**, 515–519 (2013).
8. Mykhailiuk, P. K. Saturated bioisosteres of benzene: where to go next? *Org. Biomol. Chem.* **17**, 2839–2849 (2019).
9. Stepan, F. F. et al. Application of the bicyclo[1.1.1]pentane motif as a nonclassical phenyl ring bioisostere in the design of a potent and orally active γ-secretase inhibitor. *J. Med. Chem.* **55**, 3414–3424 (2012).
10. Frank, N. et al. Synthesis of *meta*-substituted arene bioisosteres from [3.1.1]propellane. *Nature* **611**, 721–726 (2022).
11. Iida, T. et al. Practical and facile access to bicyclo[3.1.1]heptanes: potent bioisosteres of meta-substituted benzenes. *J. Am. Chem. Soc.* **144**, 21848–21852 (2022).
12. Wiesenfeldt, M. P. et al. General access to cubanes as benzene bioisosteres. *Nature* **618**, 513–518 (2023).
13. Kazi, N., Aublette, M. C., Allinson, S. L. & Coote, S. C. A practical synthesis of 1,3-disubstituted cubane derivatives. *Chem. Commun.* **59**, 7971–7973 (2023).
14. Yang, Y. et al. An intramolecular coupling approach to alkyl bioisosteres for the synthesis of multisubstituted bicycloalkyl boronates. *Nat. Chem.* **13**, 950–955 (2021).
15. Rigotti, T. & Bach, T. Bicyclo[2.1.1]hexanes by visible light-driven intramolecular crossed [2+2] photocycloadditions. *Org. Lett.* **24**, 8821–8825 (2022).
16. Levterov, V. V., Panasyuk, Y., Pivnytska, V. O. & Mykhailiuk, P. K. Water-soluble non-classical benzene mimetics. *Angew. Chem. Int. Edn* **59**, 7161–7167 (2020).
17. Levterov, V. V. et al. 2-Oxabicyclo[2.1.1]hexanes: synthesis, properties, and validation as bioisosteres of *ortho*- and *meta*-benzenes. *Angew. Chem. Int. Edn* **63**, e202319831 (2024).
18. Zhao, J.-X. et al. 1,2-Difunctionalized bicyclo[1.1.1]pentanes: long–sought-after mimetics for *ortho*/*meta*-substituted arenes. *Proc. Natl Acad. Sci. USA* **118**, e2108881118 (2021).
19. Epplin, R. C. et al. [2]-Ladderanes as isosteres for *meta*-substituted aromatic rings and rigidified cyclohexanes. *Nat. Commun.* **13**, 6056 (2022).
20. Smith, E. et al. Silver(I)-catalyzed synthesis of cuneanes from cubanes and their investigation as isosteres. *J. Am. Chem. Soc.* **145**, 16365–16373 (2023).
21. Son, J.-Y. et al. Exploring cuneanes as potential benzene isosteres and energetic materials: scope and mechanistic investigations into regioselective rearrangements from cubanes. *J. Am. Chem. Soc.* **145**, 16355–16364 (2023).

22. Fujiwara, K. et al. Biological evaluation of isosteric applicability of 1,3-substituted cuneanes as m-substituted benzenes enabled by selective isomerization of 1,4-substituted cubanes. *Chem. Eur. J.* **30**, e202303548 (2023).
23. Nguyen, L. A., He, H. & Pham-Huy, C. Chiral drugs: an overview. *Int. J. Biomed. Sci.* **2**, 85–100 (2006).
24. de Groot, C. O. et al. A cell biologist's field guide to aurora kinase inhibitors. *Front. Oncol.* **5**, 285 (2015).
25. Lake, E. W. et al. Quantitative conformational profiling of kinase inhibitors reveals origins of selectivity for Aurora kinase activation states. *Proc. Natl Acad. Sci. USA* **115**, E11894–E11903 (2018).
26. Martin, H.-D. & Mayer, B. Proximity effects in organic chemistry—the photoelectron spectroscopic investigation of non-bonding and transannular interactions. *Angew. Chem. Int. Edn* **22**, 283–314 (1983).
27. Houk, K. N. et al. Ionization potentials, electron affinities, and molecular orbitals of 2-substituted norbornadienes. Theory of 1,2 and homo-1,4 carbene cycloaddition selectivities. *J. Am. Chem. Soc.* **105**, 5563–5569 (1983).
28. Winstein, S. & Shatavsky, M. 2,6-Homoconjugate addition to bicycloheptadiene. *Chem. Ind.* **1956**, 56–57 (1956).
29. Matteson, D. S. & Waldbillig, J. O. A preferred inversion in an electrophilic displacement: mercurideboronation of *exo*- and *endo*-5-norbornene-2-boronic acids. *J. Am. Chem. Soc.* **85**, 1019–1020 (1963).
30. Tang, W. et al. Efficient monophosphorus ligands for palladium-catalyzed Miyaura borylation. *Org. Lett.* **13**, 1366–1369 (2011).
31. Liang, H. & Morken, J. P. Stereospecific transformations of alkylboronic esters enabled by direct boron-to-zinc transmetalation. *J. Am. Chem. Soc.* **145**, 9976–9981 (2023).
32. Xu, N., Liang, H. & Morken, J. P. Copper-catalyzed stereospecific transformations of alkylboronic esters. *J. Am. Chem. Soc.* **144**, 11546–11552 (2022).
33. Mlynarski, S. N., Karns, A. S. & Morken, J. P. Direct stereospecific amination of alkyl and aryl pinacol boronates. *J. Am. Chem. Soc.* **134**, 16449–16451 (2012).
34. Sadhu, K. M. & Matteson, D. S. (Chloromethyl)lithium: efficient generation and capture by boronic esters and a simple preparation of diisopropyl (chloromethyl)boronate. *Organometallics* **4**, 1687–1689 (1985).
35. Xu, N., Kong, Z., Wang, J. Z., Lovinger, G. J. & Morken, J. P. Copper-catalyzed coupling of alkyl vicinal bis(boronic esters) to an array of electrophiles. *J. Am. Chem. Soc.* **144**, 17815–17823 (2022).
36. Zhang, M., Lee, P. S., Allais, C., Singer, R. A. & Morken, J. P. Desymmetrization of vicinal bis(boronic) esters by enantioselective Suzuki–Miyaura cross-coupling reaction. *J. Am. Chem. Soc.* **145**, 8308–8313 (2023).
37. Chen, C., Hou, L., Cheng, M., Su, J. & Tong, X. Palladium(0)-catalyzed iminohalogenation of alkenes: synthesis of 2-halomethyl dihydropyrroles and mechanistic insights into the alkyl halide bond formation. *Angew. Chem. Int. Edn* **54**, 3092–3096 (2015).
38. Chen, X. et al. Pd(0)-catalyzed asymmetric carbohalogenation: H-bonding-driven C($sp^3$)–halogen reductive elimination under mild conditions. *J. Am. Chem. Soc.* **143**, 1924–1931 (2021).
39. McDonald, R. I., Liu, G. & Stahl, S. S. Palladium(II)-catalyzed alkene functionalization via nucleopalladation: stereochemical pathways and enantioselective catalytic applications. *Chem. Rev.* **111**, 2981–3019 (2011).
40. Saunders, M., Laidig, K. E. & Wolfsberg, M. Theoretical calculation of equilibrium isotope effects using ab initio force constants: application to NMR isotope perturbation studies. *J. Am. Chem. Soc.* **111**, 8989–8994 (1989).
41. Franz, D. E., Singleton, D. A. & Snyder, J. P. $^{13}$C kinetic isotope effects for the addition of lithium dibutylcuprate to cyclohexenone. Reductive elimination is rate-determining. *J. Am. Chem. Soc.* **119**, 3383–3384 (1997).
42. Kathuria, S. et al. Modulation of anxiety through blockade of anandamide hydrolysis. *Nat. Med.* **9**, 76–81 (2003).
43. Piomelli, D. et al. Pharmacological profile of the selective FAAH inhibitor KDS-4103 (URB597). *CNS Drug Rev.* **12**, 21–38 (2006).
44. Van Esbroeck, A. C. M. et al. Activity-based protein profiling reveals off-target proteins of the FAAH inhibitor BIA 10-2474. *Science* **356**, 1084–1087 (2017).
45. Chen, J. K. I only have eye for ewe: the discovery of cyclopamine and development of Hedgehog pathway-targeting drugs. *Nat. Prod. Rep.* **33**, 595–601 (2016).
46. Pan, S. et al. Discovery of NVP-LDE225, a potent and selective smoothened antagonist. *ACS Med. Chem. Lett.* **1**, 130–134 (2010).
47. Taipale, J. et al. Effects of oncogenic mutations in *Smoothened* and *Patched* can be reversed by cyclopamine. *Nature* **406**, 1005–1009 (2000).
48. Jain, N. & Yalkowsky, S. H. Estimation of the aqueous solubility I: application to organic nonelectrolytes. *J. Pharm. Sci.* **90**, 234–252 (2001).
49. Nicolaou, K. C. et al. Synthesis and biopharmaceutical evaluation of imatinib analogues featuring unusual structural motifs. *ChemMedChem* **11**, 31–37 (2016).

## Reporting summary

Further information on research design is available in the Nature Portfolio Reporting Summary linked to this article.

## Data availability

Crystal structure data for compound **20** have been deposited at the Cambridge Structure Data Centre (CCDC 2325329). Mass spectrometry proteomics data have been deposited to the ProteomeXchange Consortium through the PRIDE[50] partner repository with the dataset identifier PXD051400. All other data are available in the main text or in the Supplementary Information.

50. Perez-Riverol, Y. et al. The PRIDE database resources in 2022: a hub for mass spectrometry-based proteomics evidences. *Nucleic Acids Res.* **50**, D543–D552 (2022).

**Acknowledgements** We thank B. Li and T. Jayasundera of Boston College for assistance with X-ray structure analysis and NMR spectroscopy, respectively. Funding from the National Institutes of Health R35GM127140 (J.P.M.), R35GM127030 (J.K.C.), R35GM134694 (E.W.), S10OD026910 (Boston College), National Science Foundation MRI Award CHE2117276 (Boston College) and a Lamattina Fellowship (H.L.).

**Author contributions** M.Z. and J.P.M. conceptualized the study; M.Z. and M.C. conducted the synthetic investigation; H.L. performed the density functional theory calculations; B.X. and E.W. studied the hydrolase inhibition; B.R.S. and J.K.C. investigated the Hh inhibition; J.P.M. assisted with the writing of the initial draft; and all authors contributed to the review and editing of the paper.

**Competing interests** J.P.M., M.Z. and H.L. declare that provisional patent applications have been filed on boron-containing cyclic molecules (US provisional application 63/509,173 and international patent application PCT/US24/34873). All other authors have no competing interests.

**Additional information**

**Supplementary information** The online version contains supplementary material available at https://doi.org/10.1038/s41586-024-07865-4.

**Correspondence and requests for materials** should be addressed to James K. Chen, Eranthie Weerapana or James P. Morken.

**Peer review information** *Nature* thanks Antonia Stepan and the other, anonymous, reviewer(s) for their contribution to the peer review of this work.

nature research

Corresponding author(s): James K. Chen, Eranthie Weerapana, James P. Morken

Last updated by author(s): Mar 16, 2024

# Reporting Summary

Nature Research wishes to improve the reproducibility of the work that we publish. This form provides structure for consistency and transparency in reporting. For further information on Nature Research policies, see our Editorial Policies and the Editorial Policy Checklist.

## Statistics

For all statistical analyses, confirm that the following items are present in the figure legend, table legend, main text, or Methods section.

| n/a | Confirmed | |
|---|---|---|
| ☐ | ☒ | The exact sample size (*n*) for each experimental group/condition, given as a discrete number and unit of measurement |
| ☐ | ☒ | A statement on whether measurements were taken from distinct samples or whether the same sample was measured repeatedly |
| ☐ | ☒ | The statistical test(s) used AND whether they are one- or two-sided<br>*Only common tests should be described solely by name; describe more complex techniques in the Methods section.* |
| ☐ | ☒ | A description of all covariates tested |
| ☒ | ☐ | A description of any assumptions or corrections, such as tests of normality and adjustment for multiple comparisons |
| ☐ | ☒ | A full description of the statistical parameters including central tendency (e.g. means) or other basic estimates (e.g. regression coefficient) AND variation (e.g. standard deviation) or associated estimates of uncertainty (e.g. confidence intervals) |
| ☐ | ☒ | For null hypothesis testing, the test statistic (e.g. *F*, *t*, *r*) with confidence intervals, effect sizes, degrees of freedom and *P* value noted<br>*Give P values as exact values whenever suitable.* |
| ☒ | ☐ | For Bayesian analysis, information on the choice of priors and Markov chain Monte Carlo settings |
| ☒ | ☐ | For hierarchical and complex designs, identification of the appropriate level for tests and full reporting of outcomes |
| ☒ | ☐ | Estimates of effect sizes (e.g. Cohen's *d*, Pearson's *r*), indicating how they were calculated |

*Our web collection on statistics for biologists contains articles on many of the points above.*

## Software and code

Policy information about availability of computer code

| | |
|---|---|
| Data collection | Tecan Infinite M1000/M1000 PRO microplate reader. Mass spectrometry data was collected on an Orbitrap Exploris 240 running Thermo Scientific Xcalibur v4 |
| Data analysis | Microsoft Excel (version:16.81), Prism 9 (version:9.3.1) Mass spectrometry data was analyzed using Thermo Proteome Discoverer v2.4 running SequestHT and Percolator |

For manuscripts utilizing custom algorithms or software that are central to the research but not yet described in published literature, software must be made available to editors and reviewers. We strongly encourage code deposition in a community repository (e.g. GitHub). See the Nature Research guidelines for submitting code & software for further information.

## Data

Policy information about availability of data

All manuscripts must include a data availability statement. This statement should provide the following information, where applicable:

- Accession codes, unique identifiers, or web links for publicly available datasets
- A list of figures that have associated raw data
- A description of any restrictions on data availability

Any data generated or analyzed during this study, associated protocols, and materials are available from the corresponding author on reasonable request. Mass spectrometry data for this study will be deposited in ProteomeXchange via the PRIDE partner repository. Protein databases employed for MS/MS searches were obtained from the third party UniprotKB protein database.

# Field-specific reporting

Please select the one below that is the best fit for your research. If you are not sure, read the appropriate sections before making your selection.

☒ Life sciences ☐ Behavioural & social sciences ☐ Ecological, evolutionary & environmental sciences

For a reference copy of the document with all sections, see nature.com/documents/nr-reporting-summary-flat.pdf

# Life sciences study design

All studies must disclose on these points even when the disclosure is negative.

| | |
|---|---|
| Sample size | To determine the inhibitory potency of each compound in the SHH signaling assays, at least five biological replicates were used for each compound concentration. Three independent experiments were conducted to obtain average IC50 and s.e.m. values. These sample sizes were based on our previous experience with these assays and the number of replicates required to obtain reliable and reproducible results. For hydrolase assays, mouse brains were purchased from commercial sources, and brain homegenates from a single mouse brain were treated with the indicated concentrations of compounds |
| Data exclusions | None. |
| Replication | Descriptions of the number of replicates and error bars are included in the main text and method section. Student's t-test (two-tailed, unpaired) analysis in Prism were used to compare results and calculate P values. For hydrolase assays, the number of technical replicates has been indicated and the average ratio of each entry has been reported in supplementary data. |
| Randomization | Randomization is not relevant to our SHH signaling experiments. All samples in these assays were treated uniformly and subjected to the same data analysis procedures. |
| Blinding | The SHH signaling experiments were not blinded because the quantitative results are not subject to human biases. For hydrolase assays, blinding was not performed in this study as the proteomics measurements were collected and analyzed by computer software. |

# Reporting for specific materials, systems and methods

We require information from authors about some types of materials, experimental systems and methods used in many studies. Here, indicate whether each material, system or method listed is relevant to your study. If you are not sure if a list item applies to your research, read the appropriate section before selecting a response.

## Materials & experimental systems

| n/a | Involved in the study |
|---|---|
| ☒ | ☐ Antibodies |
| ☐ | ☒ Eukaryotic cell lines |
| ☒ | ☐ Palaeontology and archaeology |
| ☐ | ☒ Animals and other organisms |
| ☒ | ☐ Human research participants |
| ☒ | ☐ Clinical data |
| ☒ | ☐ Dual use research of concern |

## Methods

| n/a | Involved in the study |
|---|---|
| ☒ | ☐ ChIP-seq |
| ☒ | ☐ Flow cytometry |
| ☒ | ☐ MRI-based neuroimaging |

# Eukaryotic cell lines

Policy information about cell lines

| | |
|---|---|
| Cell line source(s) | Shh-LIGHT2 cells: This NIH-3T3 cell-derived line was provided by Phil Beachy (Stanford University). The generation of this line is described in Taipale et. al., Nature (2000) 406:1005-1009. |
| Authentication | We confirmed SHH ligand-dependent activation of the firefly luciferase reporter in this line. No further authentication was performed. |
| Mycoplasma contamination | The cells were not tested for mycoplasm contamination. |
| Commonly misidentified lines (See ICLAC register) | None of the misidentified lines were used in this study. |

## Animals and other organisms

Policy information about studies involving animals; ARRIVE guidelines recommended for reporting animal research

| | |
|---|---|
| Laboratory animals | One C57Bl/6 strain, 12-week-old female mouse was used in this study. Frozen C57BL/6J mouse brains were purchased from The Jackson Laboratory. |
| Wild animals | Wild animals are not involved in this study. |
| Field-collected samples | The study did not involve any field-collected samples. |
| Ethics oversight | The use of the animal was approved by Stanford University Administrative Panel on Laboratory Animal Care (Protocol Number 14145). |

Note that full information on the approval of the study protocol must also be provided in the manuscript.